An integrated traction drive with a high speed surface permanent magnet external rotor motor for electric vehicles

Vandana Rallabandi[1], Mostak Mohammad[1], Himel Barua[1],
Shajjad Chowdhury[1], Burak Ozpineci[1], Jon Wilkins[1], Lianshan Lin[2], Bidzina Kekelia[3] and J. Emily Cousineau[3]
[1]National Transportation Research Center, Oak Ridge National Laboratory, Knoxville, TN, USA
[2]Material Science and Technology Division, Oak Ridge National Laboratory, Oak Ridge, TN, USA
[3]Center for Integrated Mobility Sciences, National Renewable Energy Laboratory, Golden, CO, USA
rallabandivp@ornl.gov, mohammadm@ornl.gov, baruah@ornl.gov, chowdhuryms@ornl.gov, burak@ornl.gov
wilkinsjp@ornl.gov, linl@ornl.gov, bidzina.kekelia@nrel.gov, emily.cousineau@nrel.gov

***Abstract*—This work presents the detailed design of an outer rotor motor and integrated drive for passenger electric vehicles. The motor uses non-heavy rare earth permanent magnets and operates at a top speed of 20,000rpm. In-slot ceramic heat exchangers are utilized for the cooling of the windings. The external rotor configuration of the motor leaves a significant amount of space in the stator bore, which is leveraged for the integration of the power electronics. A high speed external rotor motor creates a number of mechanical, thermal and assembly challenges and this work presents detailed thermal, mechanical and rotordynamics analysis.**

***Index Terms*—permanent magnet motor, external rotor, rotordynamics**

I. Introduction

Electric drive systems are key components in electric vehicles (EV). Figure 1 shows the required torque-speed characteristics for an EV traction motor and it is seen that a constant power speed range 1:3 is required. Owing to their wide constant power speed range, most motors used for commercial passenger electric vehicles tend to be of the interior permanent magnet (IPM) type. Such motors, applying distributed windings and complex rotor architectures, achieve high performance along with a wide constant power speed range [1]–[3].

In contrast, this paper presents the design of an external rotor surface permanent magnet (SPM) motor for electric vehicles. This machine has concentrated windings, 18-stator slots and 16-poles and uses Halbach array surface permanent magnets (PM) (Fig. 2). The advantages of using an outer rotor architecture include: a higher airgap diameter for a given overall diameter, as well as the elimination of the need for a PM retaining sleeve in the airgap. The use of concentrated windings provides an opportunity for direct in-slot cooling of the conductors using 3D printed ceramic heat exchangers which function also as phase seperators [4]. Furthermore, the external rotor configuration leaves a significant volume of space within the stator bore which is leveraged for the integration of the power-electronics drive.

Although a significant number of papers discuss external rotor motors, many focus on in-wheel EV applications, and the operating speeds are limited [5]–[8]. Most works report on electromagnetic analysis and few focus on mechanical and thermal challenges arising from external rotor designs. A notable exception includes a high speed outer rotor motor for aviation with multiphysics analysis includibg electromagnetic, mechanical and rotordynamics analysis [9]–[11].

Multiple methods of the inverter integration with the motor have been reported in the literature - including the addition of a power electronics case on the motor, modular converter units distributed over the outer periphery of the motor housing, power electronics mounted on the stator back-iron and mounted on the end-plate [12], [13]. To the best of the authors' knowledge no detailed work has been reported on the design of a motor with the power-electronics drive integrated within the stator bore.

This paper reports on a comprehensive electromagnetic, mechanical, rotordynamics and thermal analysis for high-speed external rotor motors with the power electronics drive integrated within the stator bore. It expands on the initial work reported by the extended group of authors. [14].

II. Motor performance and motor-inverter design trade offs

A six phase motor was designed to meet the US Drive Tech Team roadmap targets of 50 kW continuous and 100 kW peak power using non-heavy rare earth permanent magnets [15]. The target power density for the motor is 50 kW/liter and for the inverter, 100 kW/liter. The materials used for different parts of the motor are listed in Table I. The magnets are

Dysprosium-free (thus non-heavy rare earth) and have a maximum operating temperature of 80°C. The motor performance at different operating conditions is shown (Table II). It is seen that the target peak power at rated speed and continuous power at the rated and maximum operating speeds are met with margins. Further details on the electromagnetic performance including, demagnetization, back emf and torque waveforms, permanent magnet segmentation etc. are provided in [14].

Although surface permanent magnet (SPM) machines such as this achieve high power density and efficiency, they lack the advantage of a wide constant power speed range (CPSR) which IPM machines inherently have. The CPSR of a machine depends on the relative magnitude of the inductances and permanent magnet flux linkage, in particular the ratio $\frac{L_d}{\psi_m}$, where L_d is the per-unit d-axis inductance, and ψ_m, the permanent magnet flux linkage [16]. Designing a surface PM machine with a wide CPSR can be achieved by reducing the permanent magnet flux linkage by increase in the airgap length and/or reducing the permanent magnet height. An increase in L_d can be achieved by increasing the slot height as well as reduction in the permanent magnet height. These modifications would lead to an increase in the motor size. It is found from finite element analysis based studies that in this case, if the motor were designed to operate in the field weakening region without inverter over-sizing, its volume would increase by 23%.

On the other hand, operation over a wide CPSR can also be achieved by inverter over-sizing, which would increase the inverter volume. This suggests that a CPSR where the combined volume of the motor and drive is minimized for a given application can be identified. The impact of over-sizing the inverter to achieve operation in the constant power region on its volume can be estimated by considering the contributions of different components to the inverter volume (Fig. 3). Volumes of heat sinks and power modules would be impacted by the inverter VA rating, however, components including gate drivers, current sensors and controllers would not be impacted much. It is found from such a study that over-sizing the inverter leads to only a 10% increase in its volume. The detailed analysis is presented in [17]. Thus, this approach of inverter over-sizing to achieve operation in the constant power speed range is used in this work. It may be noted that a major requirement of this work is to maximize the power density of the motor-drive system. The inverter is rated for 300kVA.

The maximum power capability of the motor-drive system will be achieved when both the inverter current and voltage limitations are met simultaneously, therefore a fourth operating point, designated as maximum power (Number 4) is included in Table II.

III. Inverter Design

Positioning a 300kVA inverter within a 1.3 liter space is challenging, thus the bulky components such as capacitors, modules and heat sinks were optimized. A picture of a module can be seen in Fig. 4. A single PCB board was also designed

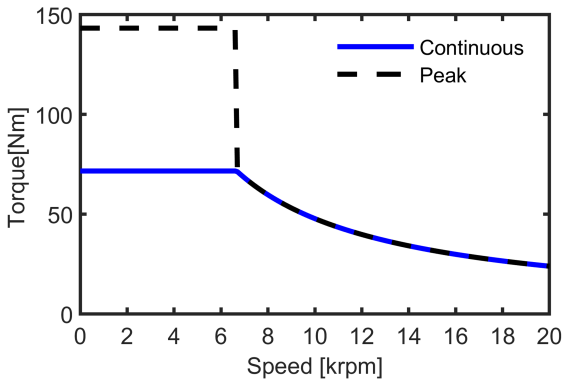

Fig. 1. Designed torque-speed characteristics.

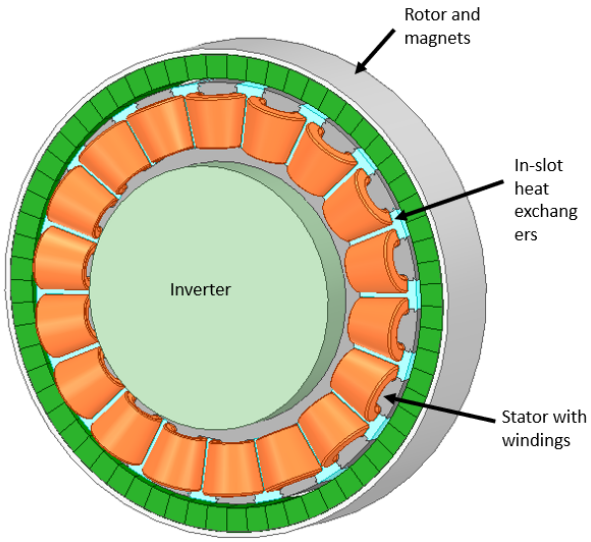

Fig. 2. Schematic of the integrated motor-drive.

containing decoupling capacitors and gate driver circuits to minimize power loop and gate loop inductance [18]. The designed PBC has limited space thus only four capacitors were added. To achieve the design capacitance value of 4.5μF [19], a secondary symmetrical capacitor board was designed and place on top of the gate driver board. The concept and advantages of the symmetrical capacitor board was presented in [19] [20]. Finally, a auxiliary circuit board was designed to house protection circuitry (i.e. shoot though and over current protection), and gate driver power supply.

A phase leg of the inverter was assembled, shown in Fig.5. The operation of the phase leg module was evaluated using a double pulse test at 800V and 150A peak current, results are shown in Fig.6. The developed module dimension was 52x52x28 mm (LxWxH) which was a perfect fit within the available space. The designed integrated electric drive assembly is shown in Fig. 7, where the inverter in integrated inside the stator bore.

TABLE I
MATERIALS USED FOR DIFFERENT PARTS OF THE MOTOR

Stator, rotor	Magnets	Rotor support	Heat exchangers	Conductors	Magnet retention
0.18mm steel	N50	17-4PH steel	Alumina	150× AWG 33 Round Litz	Carbon fiber

TABLE II
PERFORMANCE OF THE MOTOR AT THE DIFFFERENT OPERATING CONDITIONS. THE MOTOR OPERATES FROM AN 800V DC INVERTER, AND THE MAXIMUM CURRENT IS 388A.

Number.	Operating condition	Power [kW]	Current [A]	RMS Line-line voltage[V]	Copper loss [W]	Core loss [W]	Magnet loss [W]	Efficiency [%]
1	Rated Power, 6667rpm	62	194	197	699	815	27	97.6
2	Peak Power, 6667rpm	120	388	213	2798	855	31	97.01
3	Max. speed, 20,000rpm	59	194	463	699	3649	145	92.92
4	Max. power, 17500rpm	314	388	554	2798	2562	213	97.87

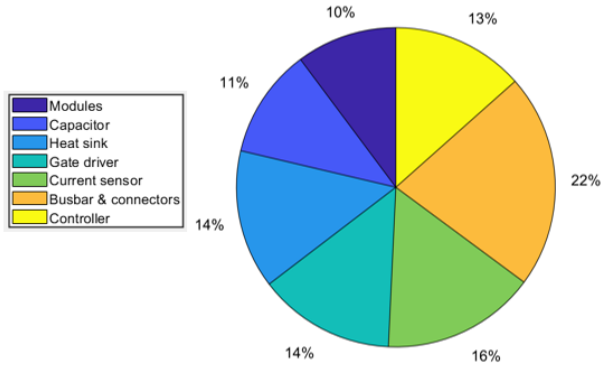

Fig. 3. Contribution of different components to the inverter volume.

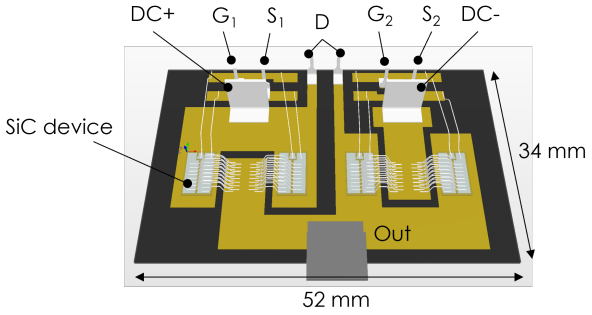

Fig. 4. Single phase power module of the inverter.

IV. MECHANICAL AND ROTOR DYNAMICS ANALYSIS

Two types of mechanical assemblies were considered for the motor - a traditional configuration supported on both sides (Fig.8) and a cantilever configuration (Fig.9). Due to the non-availability of high-speed high-bore diameter bearings, the traditional design had to be lengthened considerably in order to ensure sufficient room for the integrated power electronics inverter. Challenges arising from the design include: a) in-

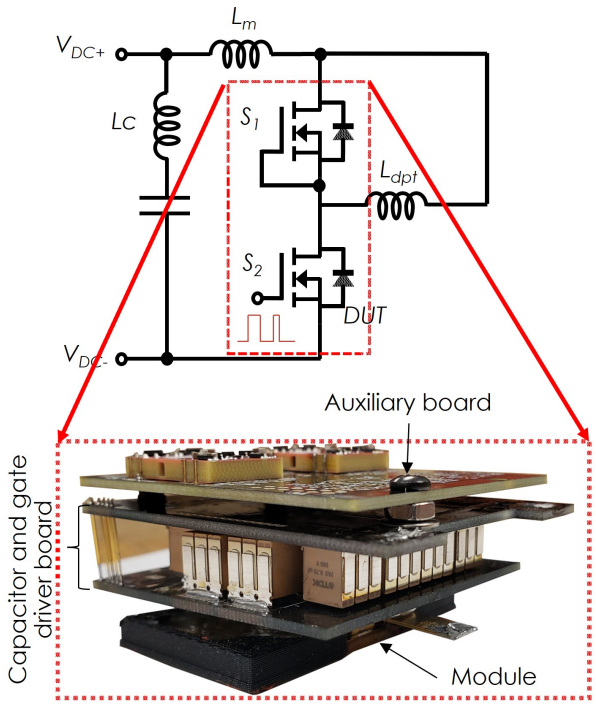

Fig. 5. Designed power module assembly and double pulse test circuit

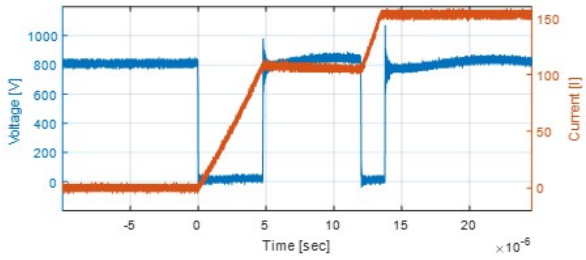

Fig. 6. Double pulse test results showing switching performance at 800V and 150A current

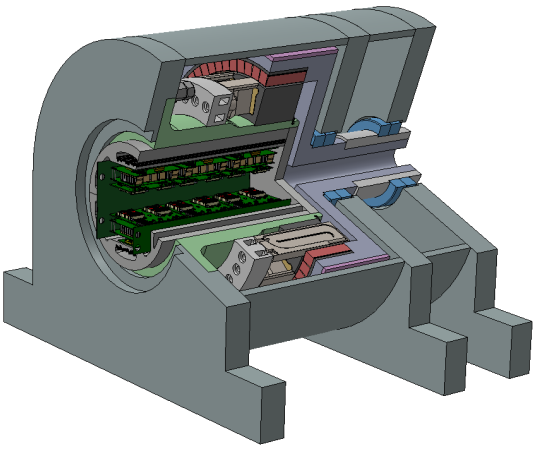

Fig. 7. Designed internal stator mount integrated electric drive

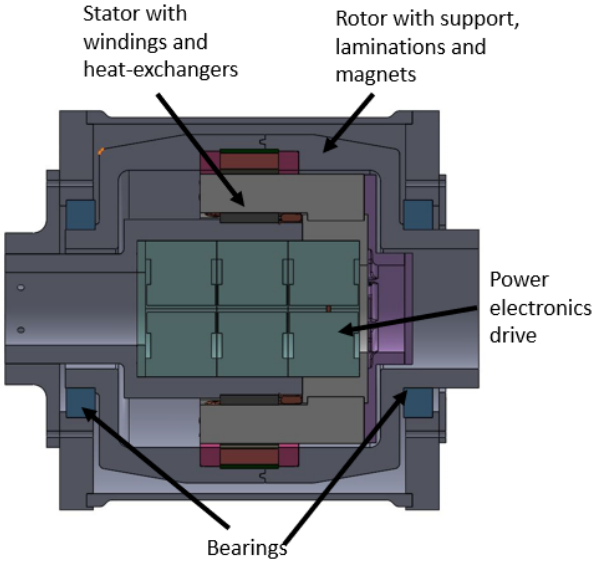

Fig. 8. The traditional assembly supported by bearings on both sides

creased length and overall weight, b) limited space within the bearing bore diameter for dc cables and fluid connections, and c) inability to remove the drive for maintenance post assembly. In order to address these limitations, a cantilever type design is also considered. However, there is a possibility for rotor dynamics challenges [11].

It was found from a 3D mechanical stress analysis con-

TABLE III
NATURAL FREQUENCIES OF THE ROTOR

Mode no.	frequency [Hz]
1	400.62
2	401.25
3	836.47
4	1743.5
5	1743.5

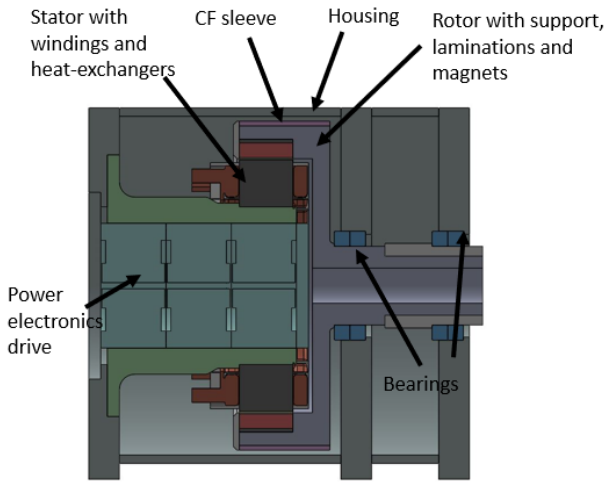

Fig. 9. The cantilever assembly supported by bearings only on one side

ducted on the rotor structure that at the top operating speed of 20,000rpm, the stresses in the permanent magnets and rotor steel far exceed their yield strength (Fig. 10 (a)). The use of a carbon fiber sleeve on the outer rotor, applying a pre-load of 100 MPa can mitigate this issue by reducing the stress in the steel and placing the magnets under compression (Fig. 10 (b)). This increases the compressive force acting on the rotor at 0 rpm (Fig. 10 (c)), however, since the permanent magnets have a much higher compressive as compared to tensile strength, the yield stresses in the rotor and magnets are well within the limits.

The first 5-modes of the rotor structure have natural frequencies ranging from 380 Hz - 1650 Hz (TableIII). The torque ripple fundamental frequency for this motor is six times the electrical frequency, which is in the range of 5.3kHz at the rated operating point. As the torque ripple frequency is much higher than the natural frequency of the rotor structure, it is expected that the modes are not excited during normal operation. The Campbell diagram for the rotor was obtained from 3D rotordynamics analysis considering a bearing stiffness of 163 $N/\mu m$. Modes 1- 3 and 5 are gyroscopic and mode 4 involves bending and axial expansion and contraction of the shaft. It shows a first critical speed of 10,000rpm. The motor would need to quickly accelerate past this speed to avoid excessive vibrations.

V. THERMAL ANALYSIS

The outer rotor design makes heat dissipation more challenging than a traditional inner rotor design. As is typical in electric motors, the stator produces the majority of heat losses. In inner rotor motors, the stator is often press fit into a cooling jacket to dissipate heat. In this design heat removal takes place at the inner surface of the stator. In fact, with the power electronics integrated into the stator cavity (Fig. 9) there would appear to be an optimized solution where the power electronics share a heat exchanger with the stator inner surface. However, this setup has a caveat. As shown in Fig. 12

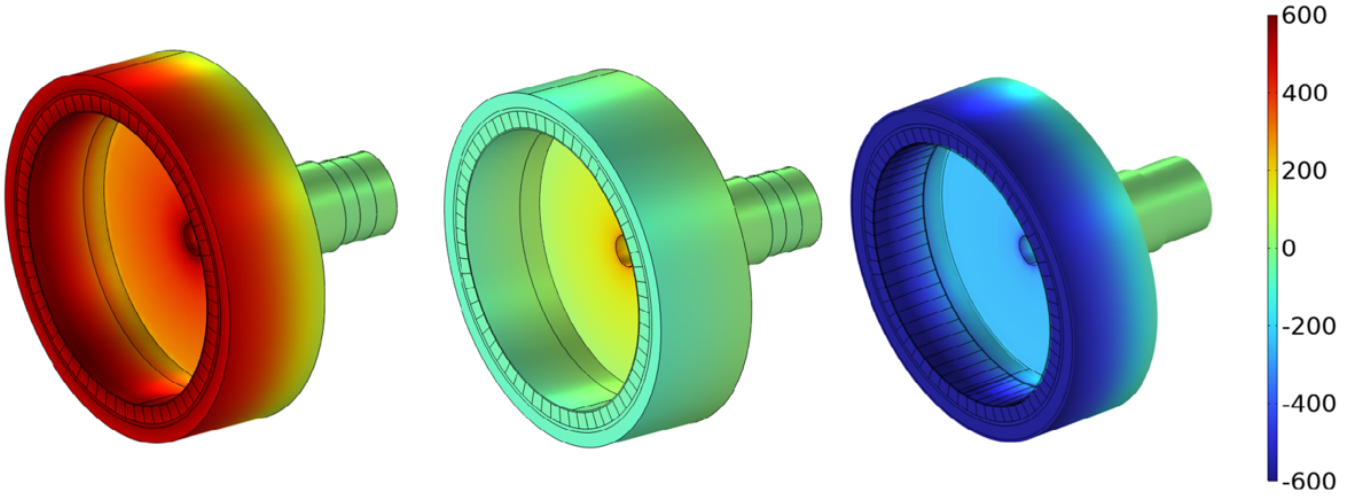

Fig. 10. Mechanical stress (MPa) on the rotor structure with (a) 20,000rpm and no pre-load, (b) 20,000 rpm with pre-load applied by the carbon fiber sleeve and (c) 0 rpm with pre-load. Positive values indicate tensile stress while negative values are compressive. With a pre-load applied, the stresses at 20,000rpm in the rotor reduce to small values. At 0 rpm, the sleeve applies compressive load on the magnets and rotor structure.

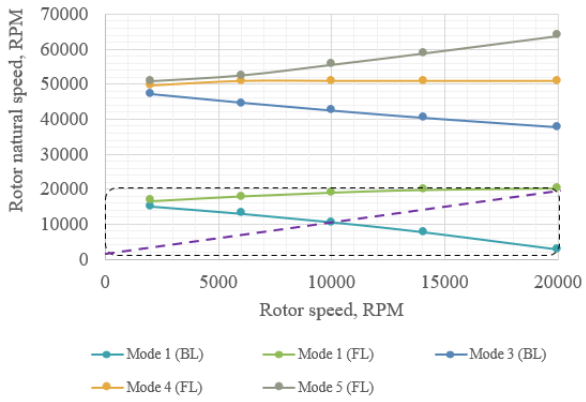

Fig. 11. Campbell diagram for the cantilever design

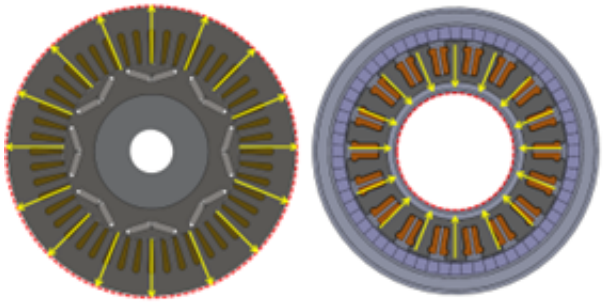

Fig. 12. Left: typical inner rotor configuration showing heat flow to its outer surface. Right: Outer rotor configuration showing heat flow to the inner surface.

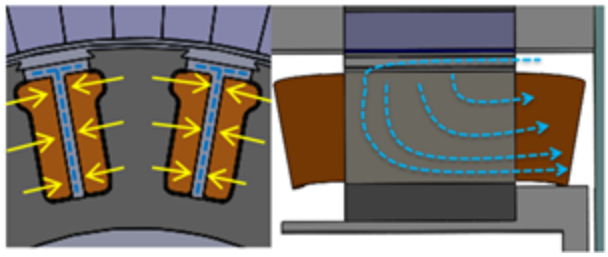

Fig. 13. Schematic of phase separator cooling concept. Left: Axial view, Right: Radial view.

there is a substantial difference surface area that can be cooled on the inner surface of this stator compared to the outer surface of a traditional inner rotor motor. Furthermore, in an inner rotor motor, the stator acts as a natural heat spreader, which facilitates a temperature gradient from the inside surface of the stator to the outside, driving heat flow. In the outer rotor configuration, heat is forced to contract as it flows to the inner surface, driving against natural dissipation.

Ultimately, it was found that inner surface cooling alone could not manage the heat loads of the stator. One solution proposed was spraying oil directly onto the end windings. However, since this motor is intended to be operated in a pure electric vehicle as opposed to a hybrid vehicle, oil is not readily available and would need to be added as a second fluid loop at the system level. Instead, the available coolant (water ethylene glycol) is brought as close as possible to the windings by flowing fluid through the phase separators, similar to [4]. Changing the interpolar slot wedge to a water-tight dielectric such as alumina enabled fluid flow very close to the temperature sensitive windings as shown in Fig. 13.

Due to complex internal channel flow of the coolant, ad-

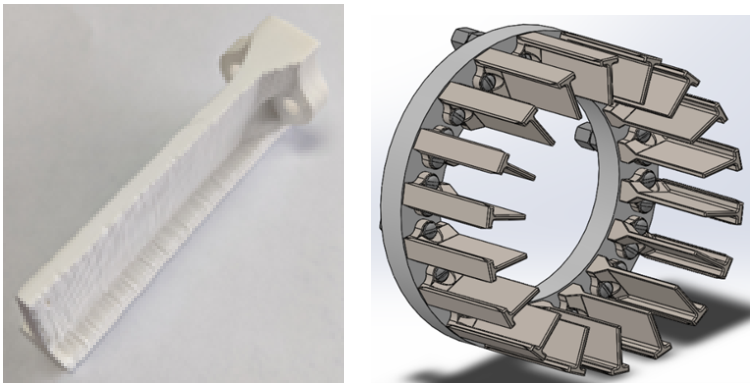

Fig. 14. (a) Prototype of a 3D printed phase separator (in-slot) heat exchanger from aluminum oxide and (b) design of the coolant distribution manifold with attached heat exchangers.

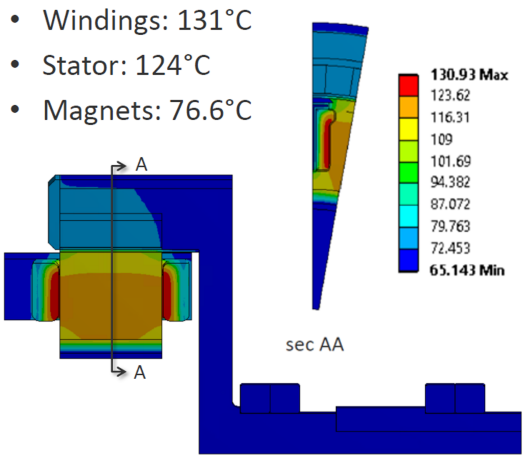

Fig. 15. Steady state temperature (°C) distribution plot at the rated condition.

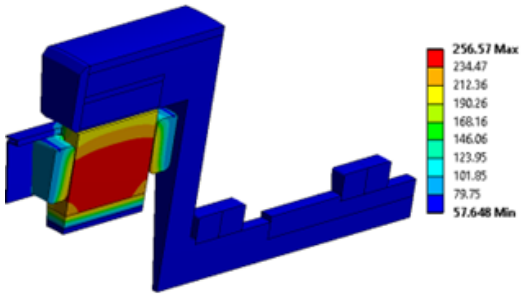

Fig. 16. Steady state temperature (°C) distribution 20,000 rpm operating point with 10 m/s airflow between the rotor and stator.

vanced manufacturing techniques (e.g. 3D printing) of the phase separator (in-slot) heat exchangers are required. Figure 14 features current design of phase separator heat exchangers and their attachment to fluid distribution manifold. The in-slot phase seperator heat-exchanger was 3d printed and a picture is shown (Fig. 14(a)).

A steady state 3D thermal analysis was conducted on the motor geometry from Fig. 9 (excluding the power-electronics converter). A half slot was simulated and the temperature plot on the longitudinal section of the motor is shown in Fig. 15. This analysis shows that the stator winding temperature well under the insulation maximum temperature. Thus, the phase seperator cooling technique proved sufficient to cool the stator.

The final remaining thermal challenge was the rotor magnet temperatures which become prohibitively high at, especially at the maximum speed operating condition. The magnets are subdivided into axial segments of 1mm thickness, thus relatively little heat is produced by the magnets. However, as previously mentioned they are Dy-free and have a maximum operating temperature of 80^oC. Furthermore, the outer rotor design causes heat to naturally dissipate from the stator into the rotor heating the rotor. As a result, the rotor temperature has a tendency to follow the stator temperature. For short transients lasting less than 5 minutes there is not a significant heat up of the rotor. However, for continuous operating points there can be significant heat flow across the airgap from the stator to the rotor.

It was found that flowing air through the gap provided significant impact to the rotor temperature. Computational fluid dynamics simulations indicated that an airspeed of 10 m/s through the airgap was sufficient to both thermally isolate the rotor from the stator, and effectively remove rotor losses even at the maximum operating speed, as shown in Fig . 16.

VI. Conclusion

This paper presents on the technical challenges of a high speed external rotor integrated motor-drive based on non-heavy rare earth permanent magnets. The inverter is proposed to be integrated within the stator bore. It is found that in order to minimize the volume of the motor-drive system, it may be advantageous to design the motor with a high magnetic loading, and to oversize the inverter to achieve the desired torque-speed characteristics. Stator cooling using in-slot ceramic heat exchangers keeps the winding temperatures below the limits, however, airgap cooling is required to maintain the magnets under the recommended operating temperature at high operating speeds. High mechanical stresses arise owing to the

high tip speed, but can be mitigated through the application of a preload using a carbon fiber sleeve. A cantilever design is proposed to simplify the assembly and allow the use of off-the-shelf bearings.

ACKNOWLEDGMENT

This material is based on work supported by the U.S. Department of Energy, Office of Energy Efficiency and Renewable Energy, Vehicle Technologies Office under contract number DE-AC05-00OR22725. The authors would like to thank the U.S. Department of Energy's Susan Rogers and National Renewable Energy Laboratory's Sreekant Narumanchi for their guidance and support.

REFERENCES

[1] F. Momen, K. Rahman, and Y. Son, "Electrical propulsion system design of Chevrolet Bolt battery electric vehicle," *IEEE Transactions on Industry Applications*, vol. 55, no. 1, pp. 376–384, 2019.

[2] I. Husain, B. Ozpineci, M. S. Islam, E. Gurpinar, G.-J. Su, W. Yu, S. Chowdhury, L. Xue, D. Rahman, and R. Sahu, "Electric drive technology trends, challenges, and opportunities for future electric vehicles," *Proceedings of the IEEE*, vol. 109, no. 6, pp. 1039–1059, 2021.

[3] Y. Zhang, W. Cao, S. McLoone, and J. Morrow, "Design and flux-weakening control of an interior permanent magnet synchronous motor for electric vehicles," *IEEE Transactions on Applied Superconductivity*, vol. 26, no. 7, pp. 1–6, 2016.

[4] W. Sixel, M. Liu, G. Nellis, and B. Sarlioglu, "Cooling of windings in electric machines via 3D printed heat exchanger," in *2018 IEEE Energy Conversion Congress and Exposition (ECCE)*, 2018.

[5] K. Reis and A. Binder, "Development of a permanent magnet outer rotor direct drive for use in wheel-hub drives," in *2014 International Conference on Electrical Machines (ICEM)*, 2014.

[6] Q. Chen, H. Shao, J. Huang, H. Sun, and J. Xie, "Analysis of temperature field and water cooling of outer rotor in-wheel motor for electric vehicle," *IEEE Access*, vol. 7, pp. 140 142–140 151, 2019.

[7] S.-U. Chung, S.-H. Moon, D.-J. Kim, and J.-M. Kim, "Development of a 20-pole–24-slot SPMSM with consequent pole rotor for in-wheel direct drive," *IEEE Transactions on Industrial Electronics*, vol. 63, no. 1, pp. 302–309, 2016.

[8] S. Yang, N. J. Baker, B. C. Mecrow, C. Hilton, G. Sooriyakumar, D. Kostic-Perovic, and A. Fraser, "Cost reduction of a permanent magnet in-wheel electric vehicle traction motor," in *2014 International Conference on Electrical Machines (ICEM)*, 2014.

[9] A. Yoon, X. Yi, J. Martin, Y. Chen, and K. Haran, "A high-speed, high-frequency, air-core PM machine for aircraft application," in *2016 IEEE Power and Energy Conference at Illinois (PECI)*, 2016.

[10] X. Yi, A. Yoon, and K. S. Haran, "Multi-physics optimization for high-frequency air-core permanent-magnet motor of aircraft application," in *2017 IEEE International Electric Machines and Drives Conference (IEMDC)*, 2017.

[11] Y. Yu, S. Sirimanna, K. Haran, T. Clydesdale, B. Sharos, D. Lubell, and B. Murphy, "Rotordynamic assessment for an inside out, high speed permanent magnet synchronous motor," in *2020 International Conference on Electrical Machines (ICEM)*, 2020.

[12] S. Chowdhury, E. Gurpinar, G.-J. Su, T. Raminosoa, T. A. Burress, and B. Ozpineci, "Enabling technologies for compact integrated electric drives for automotive traction applications," in *2019 IEEE Transportation Electrification Conference and Expo (ITEC)*, 2019.

[13] R. Abebe, G. Vakil, G. Lo Calzo, T. Cox, S. Lambert, M. Johnson, C. Gerada, and B. Mecrow, "Integrated motor drives: state of the art and future trends," *IET Electric Power Applications*, vol. 10, no. 8, pp. 757–771, 2016.

[14] T. Raminosoa, R. Wiles, J. E. Cousineau, K. Bennion, and J. Wilkins, "A high-speed high-power-density non-heavy rare-earth permanent magnet traction motor," in *2020 IEEE Energy Conversion Congress and Exposition (ECCE)*, 2020.

[15] "Electrical and electronics technical team roadmap - department of energy," 2017. [Online]. Available: https://www.energy.gov/eere/vehicles/articles/us-drive-electrical-and-electronics-technical-team-roadmap

[16] D. Ionel, J. Eastham, T. Miller, and E. Demeter, "Design considerations for permanent magnet synchronous motors for flux weakening applications," *IEE Proceedings Electric Power Applications*, vol. 145, no. 5, pp. 435–440, 1998.

[17] V. Rallabandi, S. Chowdhury, H. Barua, M. P. Paranthaman, M. Mohammad, S. Bullock, and E. Cousineau, "Traction motor design tradeoffs with additively manufactured anisotropic bonded magnets," in *2023 IEEE Transportation Electrification Conference Expo (ITEC)*, 2023, pp. 1–5.

[18] S. Chowdhury, "Integrated electric drive system," 2023, Accessed on: July 28, 2023.

[19] S. Chowdhury, E. Gurpinar, and B. Ozpineci, "Capacitor technologies: Characterization, selection, and packaging for next-generation power electronics applications," *IEEE Transactions on Transportation Electrification*, vol. 8, no. 2, pp. 2710–2720, 2022.

[20] ——, "High-energy density capacitors for electric vehicle traction inverters," in *2020 IEEE Transportation Electrification Conference Expo (ITEC)*, 2020, pp. 644–650.